ACS APPLIED MATERIALS & INTERFACES

www.acsami.org

Research Article

Enhanced Ultrasensitive Photoelectrochemical Probe for Phosphate Detection in Water Based on a Zirconium–Porphyrin Framework

Meirong Han, Weijie Zhang, Liping Lu,* Shengqian Ma,* and Sisi Feng*

Cite This: *ACS Appl. Mater. Interfaces* 2022, 14, 28280–28288

Read Online

ACCESS | Metrics & More | Article Recommendations | Supporting Information

ABSTRACT: Excessive phosphate poses a serious ecological and human health risk, and thereby, monitoring its trace concentration is of great significance to environmental protection and human health. In this work, a zirconium–porphyrin framework (PCN-222) with excellent stability and unique luminescence properties was designed to modify the surface of the indium tin oxide electrode, which was first used as a photoelectrochemical (PEC) probe for phosphate detection. The PCN-222-modified PEC probe demonstrated an excellent selectivity and stability and indicated a linear response to phosphate in the range of $0–10^6$ nM with a limit of detection (LOD) as low as 1.964 nM. To the best of our knowledge, this is the phosphate probe with the lowest LOD, and this is also the first signal-on PEC probe toward phosphate based on PCN-222. More importantly, the PEC probe can be validated for the good applicability of trace phosphate detection in real water samples, indicating a good application prospect. Finally, a series of electrochemical and spectroscopic studies have proved that phosphate can bind to the indium tin oxide (ITO)/PCN-222 electrode, which shortens the distance of the space charge region while reducing the bandwidth and thus facilitates the transfer of photogenerated electrons across the energy band barrier to reduce O_2 in the electrolyte, producing an enhanced cathodic photocurrent signal. The proposed strategy of the highly sensitive PEC probe provides a promising platform for more effective label-free phosphate monitoring in the environment and organisms.

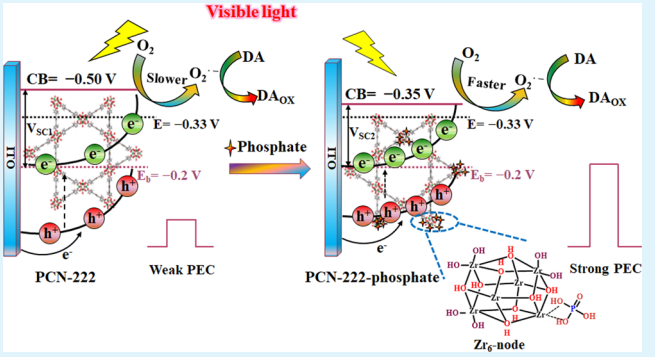

KEYWORDS: *zirconium–porphyrin MOF, PCN-222, photoelectrochemical sensing, phosphate detection, aqueous stability*

1. INTRODUCTION

The excessive presence of phosphate in aquatic environments causes eutrophication of water bodies and death of aquatic organisms and also affects the safety of human drinking water.[1−3] In this regard, phosphate has been used as an indicator to assess the water quality. On the other hand, phosphate plays an important role in many physiological processes, such as energy metabolism, bone mineralization, cell signal transduction, etc.[4−7] The level of phosphate in body fluids has been regarded as an indicator to assess individual health status, as abnormal levels of phosphate in body fluids are highly associated with various clinical diseases, including vitamin D deficiency, hypertension, hyperphosphatemia, Fanconi syndrome, hyperthyroidism, rickets, etc.[3,5,8−11] However, phosphate exhibits an orthotetrahedral structure and strong hydrophilicity and the characteristic pH-dependent morphological changes inevitably.[12] These characteristics necessarily make it difficult to selectively detect phosphates in aqueous media.[13] It is therefore essential to investigate highly specific and inexpensive detection methods for phosphate, not only from an ecological but also from a biomedical point of view.[2,14,15]

Although various techniques have been developed for the phosphate analysis, including optofluidic chips,[16] colorimetry,[17,18] chromatography,[19−21] fluorescence analysis,[1,11,17,22] and electrochemical analysis,[14,23,24] there are still some pressing drawbacks to be addressed, such as poor sensitivity, complex operation, bulky and expensive equipment, complicated sample handling, etc.[14] Photoelectrochemical (PEC) sensing combines the advantages of both electrochemical and photochemical sensing. PEC sensing is simple, inexpensive, and portable. On the other hand, the excitation source and the detection signal use two different energies, and they are completely independent, which greatly reduces the background noise and provides higher detection sensitivity.[25−27]

In recent years, several fluorescence sensing platforms based on metal–organic frameworks (MOFs) have been developed and widely used for the detection of phosphates.[2,17,28] Among

Received: March 15, 2022
Accepted: May 30, 2022
Published: June 10, 2022

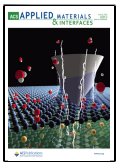

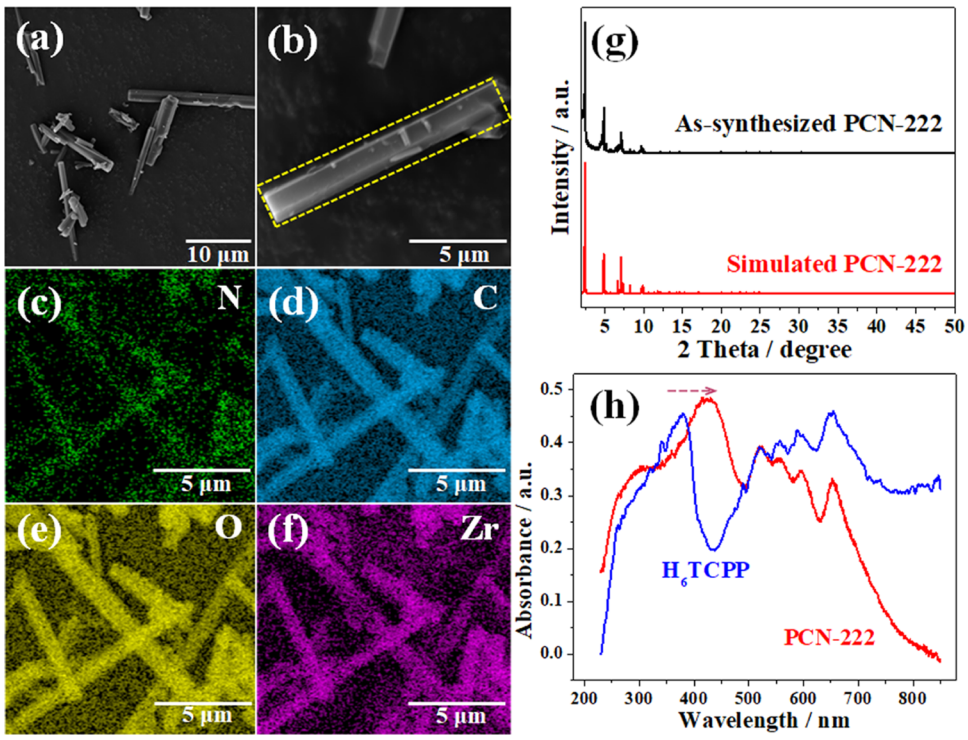

Figure 1. (a, b) SEM images and (c–f) corresponding EDS mappings of PCN-222; (g) PXRD patterns of simulated and as-synthesized PCN-222; and (h) ultraviolet–visible (UV–vis) diffuse reflectance spectra of H_6TCPP and PCN-222.

them, Zr–porphyrin MOFs synthesized from tetra(4-carboxyphenyl)porphyrin (H_6TCPP) have attracted much attention for their excellent stability and unique luminescence properties.[1,17] Due to the strong affinity between Zr^{4+} ions and phosphates, zirconium nodes and porphyrin ligands can act as recognition active sites and signal reporter groups for phosphates, respectively, in Zr-TCPP-MOFs, enabling quantitative detection by fluorescence. Inspired by the excellent PEC activity of porphyrins and the high specific surface area and outstanding aqueous stability of Zr-MOFs, Zr-TCPP-MOF materials are expected to achieve better photoelectrochemical sensing applications in aqueous media.[29]

Based on the above-mentioned discussion, a porous zirconium–porphyrin MOF with the formulation $[Zr_6(\mu_3\text{-}OH)_8(OH)_8(H_2TCPP)_2]$ (PCN-222) was selected as an electrode material. PCN-222 has been widely studied in application fields such as catalysis,[30−34] adsorption and separation,[35−40] drug delivery,[41] and chemical sensing[29,42,43] due to its excellent structure and properties. PCN-222 has both photoelectric activity and chemical binding property, and we constructed it as an ultrasensitive PEC probe for phosphate detection. The probe can be used to detect phosphate in natural water. The mechanism of PEC detection was investigated by a series of spectroscopic and electrochemical characterizations. This work provides a new idea for water eutrophication monitoring and supports the development of PEC probes for phosphate.

2. EXPERIMENTAL SECTION

2.1. Material and Characterization (Section 1 in the Supporting Information). 2.2. Synthesis of PCN-222. PCN-222 was synthesized according to the method reported in the literature.[44,45] The purple hexagonal rod-shaped PCN-222 crystals were collected by high-speed centrifugation and washed with *N*,*N*-dimethylformamide (DMF, 5 × 20 mL). The DMF was subsequently exchanged with acetone (3 × 20 mL) and stirred at 60 °C for 3 days. After the removal of acetone by centrifugation, the PCN-222 sample was activated in vacuum for 12 h at 120 °C.[46]

2.3. Preparation of ITO/PCN-222. First, indium tin oxide (ITO) electrodes (15 × 45 × 2.2 mm^3, 7.0 Ω) were cleaned sequentially with acetone, ethanol, and ultrapure water by ultrasonication for 30 min and dried under nitrogen for use. The PCN-222 suspension was prepared by mixing a 2.0 mg sample and 1.0 mL of ethanol and stored at 4 °C. A total of 15.0 μL of the suspension was coated on the ITO surface into a circle with a diameter of 0.6 cm and dried at room temperature, obtaining ITO/PCN-222 electrodes. In addition, the H_6TCPP-modified ITO (ITO/H_6TCPP) electrode was prepared according to the same procedure for comparison.

2.4. Study of the PEC Performance of ITO/PCN-222. The as-prepared ITO/PCN-222 electrode was incubated in 4-(2-hydroxyerhyl)piperazine-1-erhanesulfonic acid (HEPES) buffer solution (10 mM, pH = 6.8) containing different common ions (K^+, Na^+, Mg^{2+}, Cd^{2+}, CO_3^{2-}, Ac^-, Cl^-, SO_4^{2-}, NO_3^-, MnO_4^-, $Cr_2O_7^{2-}$, ClO_3^-, H_2O_2, glucose, glutathione, phosphate, 1.0 μM) for 2 h at room temperature. The electrode was washed with HEPES buffer and then transferred to a three-electrode cell for photocurrent signal measurements. Moreover, the xenon light source was switched on and off and irradiated cyclically (at 30 s intervals) until the photocurrent stabilized. Finally, the ITO/PCN-222 electrode produced a PEC signal in an air-saturated HEPES solution (10 mM, pH = 6.8) containing 0.01 mM dopamine (DA) as the electron donor at room temperature. DA is a small-molecule neurotransmitter, which can serve as an electron donor for photoactive materials.[29] As shown in Figure 6, oxidation of DA promoted more electrons to transition to the conduction band of PCN-222, effectively inhibiting the recombination of electron–hole pairs and promoting the continuous and stable generation of photocurrent.

2.5. Phosphate Detection in Real Water Samples. Real water samples (tap water and drinking water, collected in Shanxi University) were pretreated with 0.22 μm membrane filters to remove solid substances, and then, the phosphate concentrations in these two spiked water samples were detected using ITO/PCN-222. The detailed detection process in real samples was similar to that in

https://doi.org/10.1021/acsami.2c04645
ACS Appl. Mater. Interfaces 2022, 14, 28280−28288

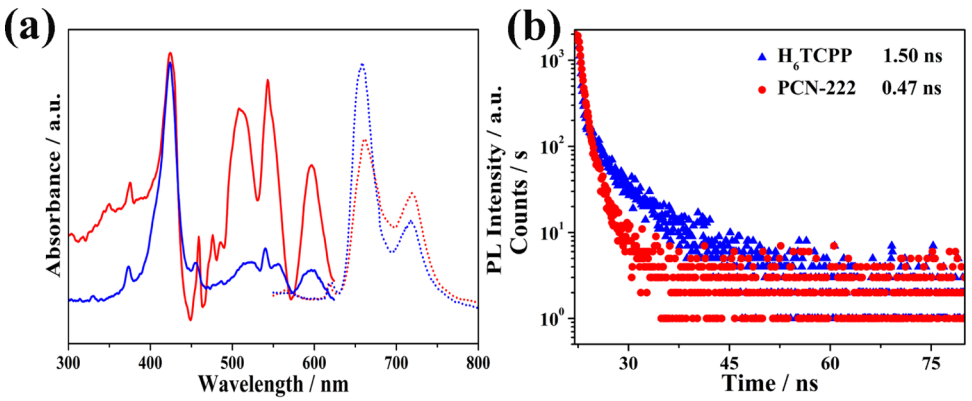

Figure 2. (a) Excitation (solid line) and photoluminescence (PL) emissions (dashed line) (λ_{ex} = 430 nm) of H_6TCPP (blue) and PCN-222 (red). (b) The lifetime decay curves of H_6TCPP and PCN-222 monitored at 660 nm under excitation at 430 nm.

Section 2.4. Three parallel experiments were performed at each concentration.

3. RESULTS AND DISCUSSION

3.1. Characterization of PCN-222. A series of characterizations were carried out to confirm the structure of PCN-222. The synthesized PCN-222 exhibited a three-dimensional hexagonal rod-like structure with a smooth surface and a scale of micrometers (Figure 1a,b). The scanning electron microscopy−energy dispersive spectroscopy (SEM-EDS) mappings of PCN-222 revealed the homogeneous distribution of the elements C, N, O, and Zr in PCN-222 (Figure 1c−f). As shown in Figure 1g, the main powder X-ray diffraction (PXRD) peaks of PCN-222 were 2.48, 4.87, 7.14, and 9.71°. The PXRD pattern closely matched with the simulation one, which is also consistent with the experimental one in the literature.[17,47] The porosity of PCN-222 has been measured by N_2 adsorption−desorption experiments at 77 K (Figure S1). The prepared PCN-222 samples showed typical type IV N_2 sorption isotherms and gave a Brunauer−Emmett−Teller (BET) surface area and total pore volume of 2233 $m^2\ g^{-1}$ and 1.652 $cm^3\ g^{-1}$, respectively, suggesting their mesoporosity. In addition, the evaluation of the density functional theory (DFT) simulation of the N_2 sorption curve revealed two types of pores with pore diameters of 1.3 and 3.2 nm, assigned to the triangular microchannel and hexagonal mesochannel, respectively (Figure S1, inset). These results proved the successful preparation of PCN-222. The highly regular porous structure and high-density channels enable PCN-222 to possess high gas storage capacity and enrichment capacity of the reaction substrate. As illustrated in Figure S2, the thermogravimetric analysis (TGA) curve showed that PCN-222 can maintain thermal stability up to 415 °C. Such excellent thermal stability can be attributed to the strong Zr−O coordination bond with H_2TCPP^{4-} in PCN-222.

Subsequently, we studied the spectral properties of PCN-222. As shown in Figure 1h, porphyrin exhibits strong absorption in the 380−450 nm region (Soret band) and weak absorption in the region of 500−700 nm (Q band),[1,17,48,49] which can also be observed in the UV−vis diffuse reflectance spectrum (UV−vis DRS) of PCN-222. However, the Soret band absorption of PCN-222 was red-shifted in comparison with that of free H_6TCPP, which may be due to the ligand-to-metal charge transfer (LMCT) interaction between H_6TCPP and the Zr−O cluster. It means not only that PCN-222 has a smaller highest occupied molecular orbital−lowest unoccupied molecular orbital (HOMO−LUMO) band gap, which is more favorable for the photoinduced electron transfer process.[29] PCN-222 can also be easily excited by visible light, which is consistent with the emission spectrum of the porphyrin ligand (Figure 2a).[30] The attenuated photoluminescence[50] intensity (Figure 2a) and the reduced fluorescence decay lifetime (Figure 2b) of PCN-222 both indicated more efficient photoelectron−hole pair separation and faster interface charge transfer compared with H_6TCPP.[30,48,51,52] It is well-known that porphyrins are widely used in the field of photoelectric analysis due to their excellent photoelectric activity.[53,54] However, the PEC properties of PCN-222 have rarely been studied.

3.2. Analytical Performance of the PEC Probe. *3.2.1. Stability and Selectivity of the PEC Probe.* A prerequisite for highly sensitive PEC detection is the generation of strong and stable photocurrent signals from the photoactive electrode. Therefore, the photocurrent response of the constructed ITO/PCN-222 PEC probe was investigated under optimal conditions (Section 1 in the Supporting Information), and the stability of the ITO/PCN-222 electrode has been investigated first by recording the photocurrent response. It can be observed in Figure 3a that the photocurrent signal generated by PCN-222 was approximately three times higher than that of the free porphyrin ligand at the same molar concentration, which indicated that the PEC activity was effectively enhanced when H_6TCPP was assembled into the MOF structure. This is because (a) the smaller HOMO−LUMO band gap of PCN-222 is more favorable for photogenerated charge transfer compared to porphyrin ligands;[30] (b) the extended conjugation in the PCN-222 framework facilitates the separation of photogenerated electron−hole pairs, thereby improving the photoelectric conversion efficiency; and (c) the larger specific surface area and three-dimensional porous structure in PCN-222 enrich dissolved oxygen and reaction substrates, thus improving the photovoltaic performance.[29,30,34] Furthermore, the photocurrent response of the ITO/PCN-222 electrode showed no significant attenuation after 36 on/off irradiation cycles for 36 min with a relative standard deviation (RSD) of 1.28%. In addition, the RSD of the photocurrent responses of the six individual ITO/PCN-222 photoelectrodes was as low as 1.63%. The results reveal that the PEC probe has the perfect stability, good reproducibility, and potential application (Figure 3b,c).

https://doi.org/10.1021/acsami.2c04645
ACS Appl. Mater. Interfaces 2022, 14, 28280−28288

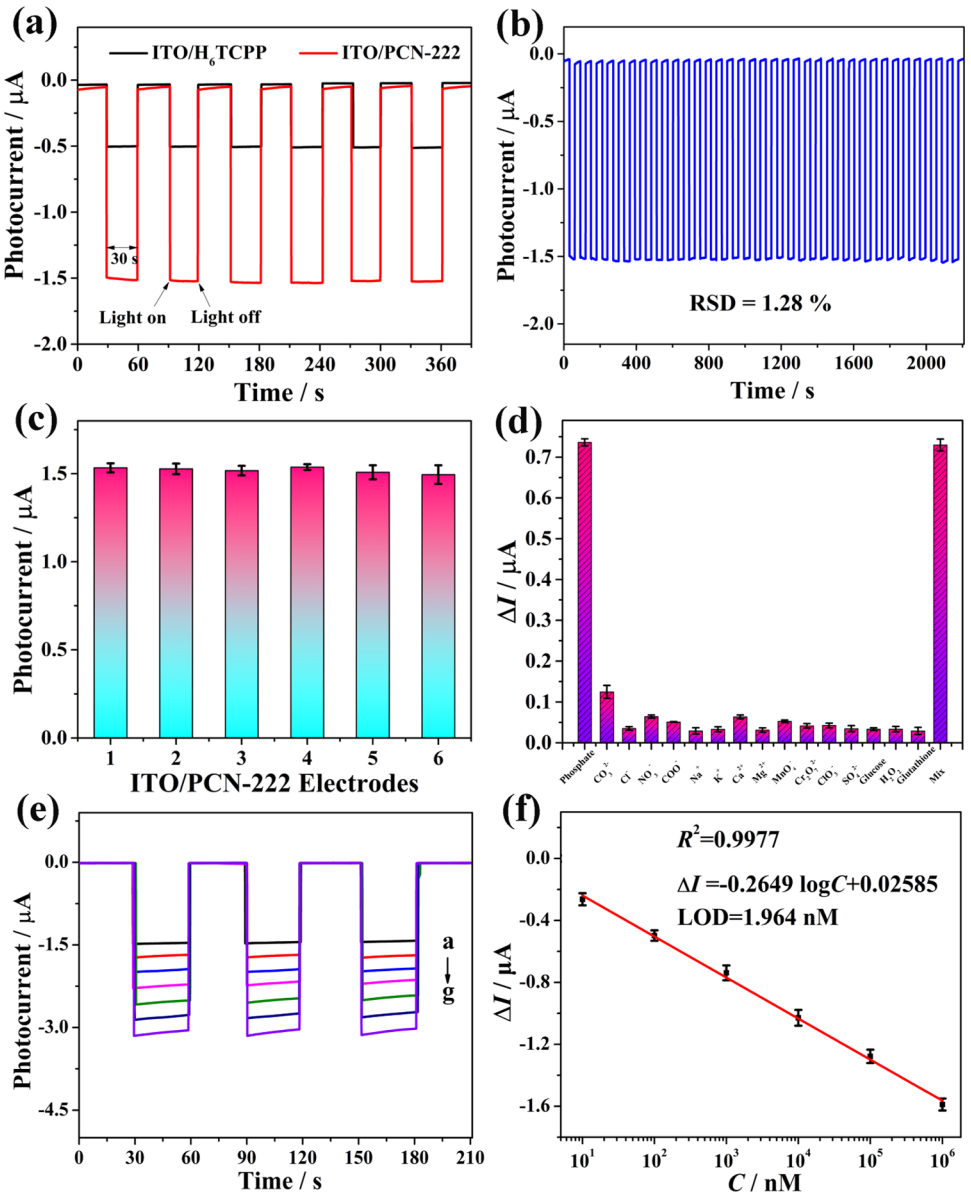

Figure 3. (a) Photocurrent responses of H_6TCPP and PCN-222 in 10 mM HEPES buffer containing 0.01 mM DA at a biased potential of 0.0 V *vs* Ag/AgCl. (b) Stability and reproducibility test in a 10 mM HEPES electrolyte under repeated on/off cycles. (c) Reproducibility of the ITO/PCN-222 electrode. (d) Selectivity and anti-interference of the ITO/PCN-222 electrode to phosphate and different interferers (the detection concentration was 1.0 μM). (e) Photocurrent response and (f) linear fitting of ITO/PCN-222 to different concentrations of phosphate, (a−g: 0, 10, 10^2, 10^3, 10^4, 10^5, 10^6 nM).

Second, the selectivity of the ITO/PCN-222 electrode as a PEC probe was investigated by measuring the photocurrent in HEPES buffer solution (10 mM, pH = 6.8) containing phosphate and other common species with the same concentration (1.0 μM) (Figure 3d). Inspiringly, the ΔI of ITO/PCN-222 electrode toward phosphate was much higher than that of other substances, and other substances cannot interfere with the detection of phosphate by the ITO/PCN-222 electrode when they were mixed together. The results demonstrated that PCN-222 as the PEC probe possesses excellent selectivity and anti-interference performance to phosphate, which may be attributed to the specific and strong binding between PCN-222 and phosphate.

3.2.2. Sensitive Performance of the PEC Probe. As shown in Figure 3e, the photocurrent signal increased gradually with the increase of the phosphate concentration. Additionally, a linear relationship was found between ΔI and the logarithm of the phosphate concentration in the range of 0−10^6 nM, where ΔI is the difference between the photocurrent before (I_0) and after (I) incubation with phosphate (Figure 3e). The linear regression equation is $\Delta I = -0.2649 \log C + 0.02585$ (R^2 = 0.9952) with a limit of detection (LOD) as low as 1.964 nM (3σ/slope) (Figure 3f). To the best of our knowledge, this is the probe for phosphate with the lowest LOD, and this is also the first signal-on PEC probe toward phosphate based on PCN-222 (Table S1). Moreover, the LOD was far lower than the detection requirements of the phosphate emission standard in the aqueous environment (6.4−320 μM),[55] that is, the PEC probe is sufficient to accurately detect phosphate in the aqueous environment and even in organisms.

3.2.3. Reproducibility, Solvent Adaptability, Long-Term Stability, and Reusability. Reproducibility is also an

https://doi.org/10.1021/acsami.2c04645
ACS Appl. Mater. Interfaces 2022, 14, 28280−28288

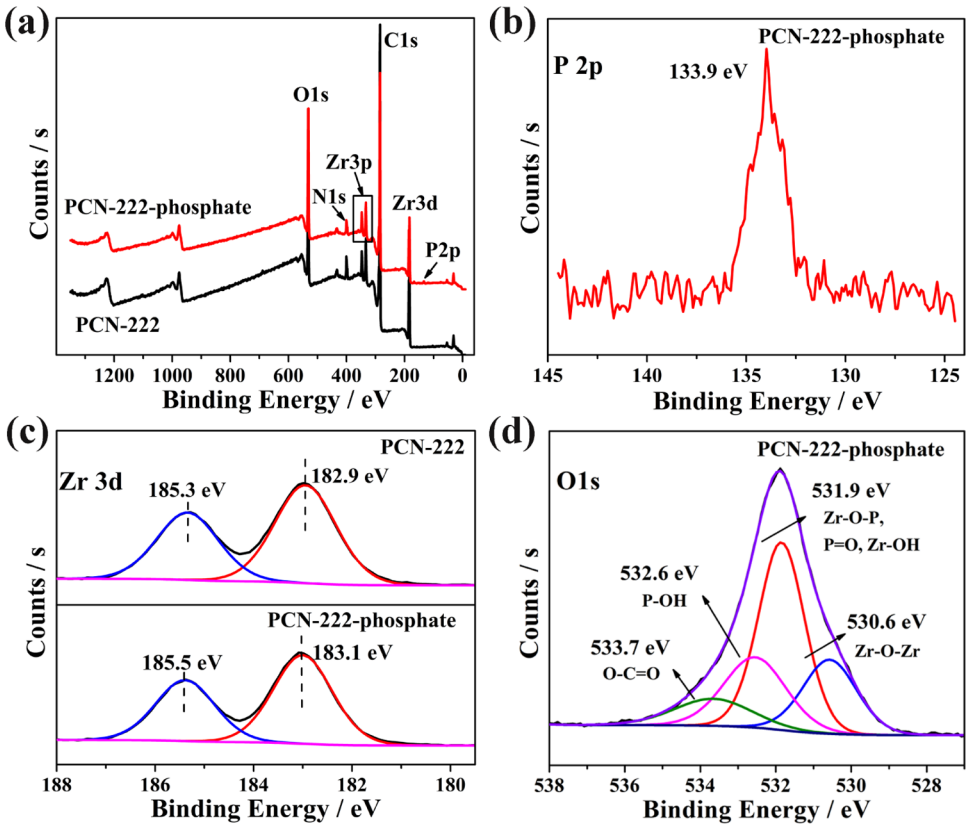

Figure 4. (a) XPS survey scans and the high-resolution XPS spectra of (b) P 2p, (c) Zr 3d, and (d) O 1s for PCN-222 and PCN-222-phosphate.

indispensable indicator for probes. The photocurrent responses of six prepared ITO/PCN-222 in detecting the same concentration of phosphate are shown in Figure S4a. The photocurrent signal deviations among six samples were very small, and the RSD for detecting 10^4 nM phosphate was 3.52%, which proves the good reproducibility of the proposed probe. In addition, the PEC probes prepared from PCN-222 after incubation in ethanol, acetone, DMF, and acetonitrile for 30 min showed good solvent adaptability. They can retain the original signal response (Figure S4b) when the same concentration of phosphate was detected. As expected, the response signal intensity of the probe can retain almost the initial value after detecting the same concentration of phosphate when the probe has been stored at 4 °C for 20 days (Figure S4c). In addition, the reusability of this PEC probe was also investigated by photocurrent testing. After 10 min of incubation in HEPES (10 mM, pH = 6.8) solution containing 15.0 μM Eu^{3+}, the photocurrent response of the PEC probe is shown in Figure S4d. More than 85% of the initial response can be observed after four repetitions, based on the strong coordination of Eu^{3+} with phosphate to regenerate the probe. These results demonstrate the excellent reproducibility, solvent adaptability, long-term stability, and reusability of the proposed PEC probe. Therefore, the probe should have a good application prospect.

3.3. Application of the PEC Probe in Real Water Samples. The practical application of the proposed PEC probe was performed in different spiked water samples (*i.e.*, tap and drinking water). As listed in Table S2, the recoveries of spiked samples ranged from 96.86 to 102.87% with ~2.0% RSD. These results showed that the proposed PEC probe can be used to detect phosphate in real water samples with excellent selectivity, accuracy, and reliability.

3.4. PEC Sensing Mechanism for Phosphate Detection. *3.4.1. Study on the Interaction between PCN-222 and Phosphate.* First, the ITO/H_6TCPP electrode was prepared by the same method, and the PEC detection of phosphate was performed as the control experiment. The results shown in Figure S5 indicated that the ITO/H_6TCPP-modified electrode did not respond to the phosphate. Moreover, the P element was homogeneously distributed as the Zr element in the skeleton (Figure S6d,e), indicating an ideal binding capacity of PCN-222 toward phosphate. Interestingly, the PXRD patterns of PCN-222 before and after phosphate detection revealed that the original skeleton structure was still preserved (Figure S7), which confirmed the good stability of the PCN-222 frame throughout the detection process.

Then, Fourier transform infrared spectroscopy (FT-IR) and X-ray photoelectron spectroscopy (XPS) were carried out to further explore the interaction between PCN-222 and phosphate.

As shown in Figure S8, the strong peak at 3421 cm^{-1} in FT-IR spectra should correspond to the ν(OH) stretching vibration of the carboxyl and water molecules for the original PCN-222. The characteristic peaks at 1599 and 1382 cm^{-1} were attributed to the ν_{as}(COO) and ν_s(COO) vibrations of the H_6TCPP ligand, respectively, and the characteristic peak near 1544 cm^{-1} was attributed to the C=C vibration peak of aromatic rings.[1,56,57] The peaks in the range of 800−600 cm^{-1} were attributed to Zr−O_2 in the longitudinal and transverse modes.[57,58]

After phosphate detection, it was observed that the characteristic peak of phosphate appeared at 1100−890

https://doi.org/10.1021/acsami.2c04645
ACS Appl. Mater. Interfaces 2022, 14, 28280−28288

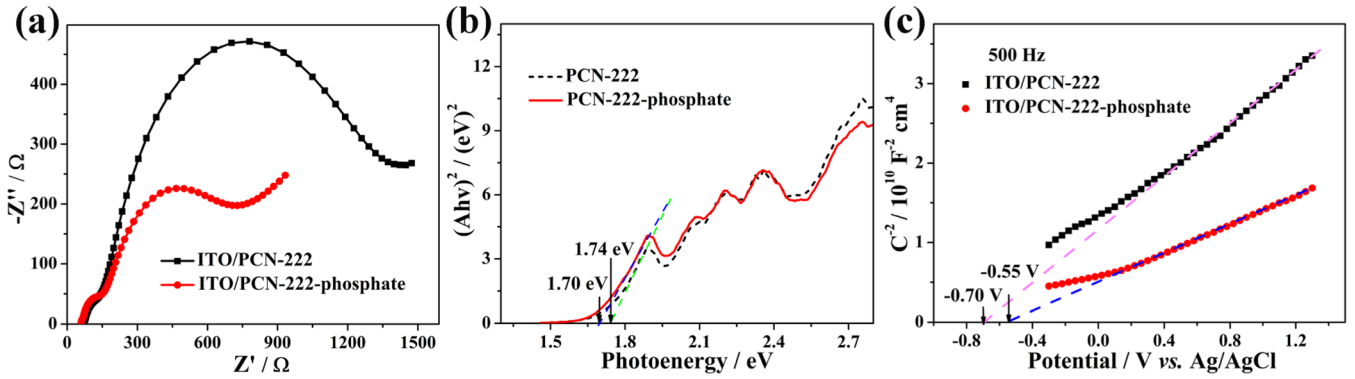

Figure 5. (a) Nyquist plots, (b) Tauc plots, and (c) Mott−Schottky plots of ITO/PCN-222 before and after PEC detection of phosphate.

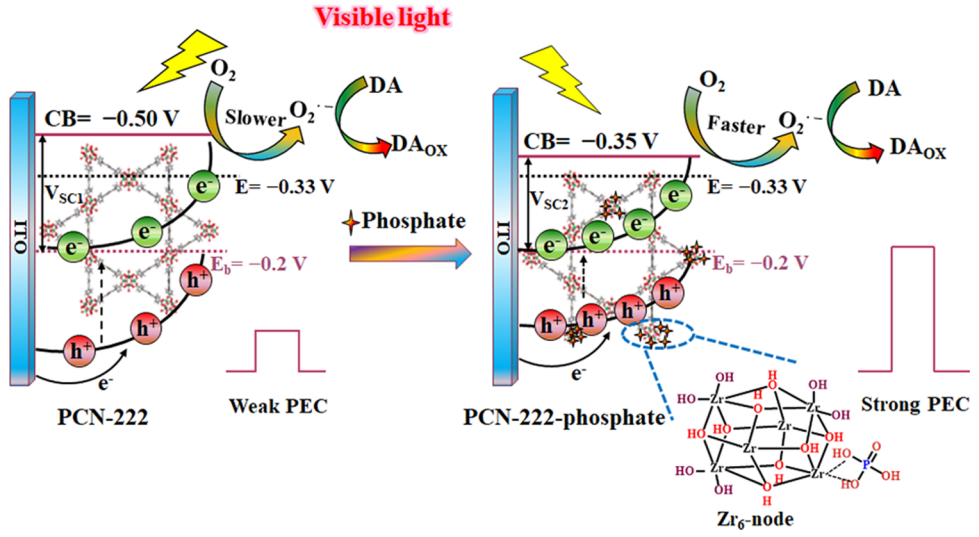

Figure 6. Mechanism of photocurrent enhancement through the ITO/PCN-222 electrode combined with phosphate (E/V *vs* NHE).

cm^{-1}.[1,4,55] Among them, there were strong absorption peaks at 1100 and 1016 cm^{-1}, suggesting the formation of the P═O and P−OH bonds, respectively. The shoulder peak at 968 cm^{-1} attributed to the P−O−Zr bond was red-shifted compared to that of the single phosphate,[4,56] demonstrating that the Zr−OH group in PCN-222 may specifically bind to phosphate through the formation of a Zr−O−P coordination bond.[56]

The XPS spectra of PCN-222 before and after phosphate detection are shown in Figure 4. Except for C, N, O, and Zr elements, the new P 2p peak at 133.9 eV can be observed in the spectra (Figure 4a,b), which indicated that the phosphate was successfully bound to the PCN-222 framework.[29,56] Moreover, in the Zr 3d spectra, two peaks at 182.9 and 185.3 eV (corresponding to Zr $3d_{5/2}$ and Zr $3d_{3/2}$, respectively) were derived from the coordination between Zr−O clusters and carboxylic groups of the porphyrin ligand.[55,56,59] They shifted to 183.1 and 185.5 eV, respectively, after binding with phosphate, due to the partial loss of Zr 3d charge density caused by the combination of the strong electronegative P−O bonds (Figure 4c).[55,60] Meanwhile, the O 1s spectra can be divided into four peaks (Figure 4d), which might be ascribed to O in Zr−O−Zr (530.6 eV), P═O and Zr−O−P (531.9 eV), P−O−H (532.6 eV), and O−C═O (533.7 eV).[55−57] The above-mentioned analyses indicated a strong complexing effect between PCN-222 and phosphate, which was consistent with the FT-IR results.

3.4.2. Mechanism of Phosphate-Induced PEC Signal Enhancement. There was no obvious change in the surface morphology of PCN-222 before and after phosphate detection (Figure S6a−c). Therefore, the change of photocurrent was not due to the corrosion of the electrode surface. To further understand the mechanism of photoelectric conversion by the ITO/PCN-222 electrode, more controls were investigated. It can be observed from Figure S9 that the photocurrent of the ITO/PCN-222 electrode increased significantly with the addition of O_2 in the electrolyte solution, demonstrating that O_2 plays a key role in the cathodic photocurrent reaction of the ITO/PCN-222 electrode. Because the electrons generated by the photoexcitation are transferring from the valence band (VB) to the conduction band (CB) in PCN-222,[61] they can reduce the dissolved O_2 to produce superoxide radicals ($O_2^{\bullet-}$) and then facilitate the generation of cathode reduction current.[59] In short, the dissolved O_2 can receive electrons from PCN-222 to generate $O_2^{\bullet-}$, during photoexcitation.

Subsequently, electrochemical impedance spectroscopy (EIS), UV−vis DRS, and Mott−Schottky curves were used to explore the mechanism of PEC signal enhancement after phosphate binding (Section 3 in the Supporting Information). As shown in Figure 5a, the radius of the impedance curve of ITO/PCN-222 after combination of phosphate was significantly reduced, indicating smaller charge transfer resistance and faster electron mobility.[62]

https://doi.org/10.1021/acsami.2c04645
ACS Appl. Mater. Interfaces 2022, 14, 28280−28288

It is well-known that the physical parameters of the semiconductor, such as forbidden bandwidth, the position of the band gap, and the carrier concentration, are important factors for the occurrence of PEC reactions.[59] The Tauc plot obtained from the UV−vis DRS is usually used to determine the band gap energy of a semiconductor (Section 3 (I) in the Supporting Information).[63] As shown in Figure 5b, the band gap of the PCN-222 (1.74 eV)[30] was reduced to 1.70 eV when it was combined with phosphate, demonstrating the improved light absorption capacity of the material and the enhanced photocurrent.

In addition to the forbidden bandwidth, the effects of the ITO/PCN-222 band gap position and conductive type on photocurrent variation were also investigated. Mott−Schottky measurements of PCN-222 before and after phosphate detection were performed at a frequency of 500 Hz (Figure 5c). The positive slopes of Mott−Schottky plots for both electrodes were consistent with the typical n-type semiconductor. The flat band potential (V_{fb}) of the ITO/PCN-222 electrode calculated according to the Mott−Schottky diagram shifts from −0.50 V (*vs* NHE) to −0.35 V (*vs* NHE) after binding phosphate (Figure 5c). According to the carrier density N_A formula, the significantly increased N_A indicated accelerated charge transfer and enhanced PEC signal (Figure 6) (Section 3 (II, III) in the Supporting Information).[62] Moreover, the energy band bends upward when the n-type semiconductor is in contact with the electrolyte based on the principle of semiconductor electrochemistry.[59] As shown in Figure 6, a "built-in" electric field was formed at the interface between the semiconductor and the electrolyte, and the direction of the electric field was from the electrode to the electrolyte, which may hinder the transfer of electrons from the electrode surface to the electrolyte. However, the generation of a photocurrent signal indicated that a certain amount of electrons could be transferred across the barrier to the oxygen in the electrolyte to form a cathode photocurrent. Taking into account the existence of the "built-in" electric field, the narrower its space charge region (SCR) was, the easier it was for the electrons to cross the barrier and transfer to oxygen and thus, the higher the photocurrent was.[59] As shown in Figure 6, since the bias voltages of ITO/PCN-222 and ITO/PCN-222-phosphate were set to be 0.0 V *vs* Ag/AgCl (*i.e.*, −0.2 V *vs* NHE) during the measurement, the energy band bending degree of ITO/PCN-222 was 0.70 V, greater than the 0.55 V of PCN-222-phosphate. Therefore, it can be concluded that the thickness of the SCR formed by the modified electrode becomes narrower under the action of phosphate.

For the mechanism study, the narrower space charge layer facilitated the transfer of more electrons through the interfacial electric field to the electrolyte to reduce oxygen at a redox potential of −0.33 V (*vs* NHE) (Figure 6).[64] Thus, the cathode photocurrent detected through the probe was due to the reduction of O_2 by photoinduced electrons. Phosphate binding shortens the distance of the SCR while reducing the bandwidth, makes it easier for the photogenerated electrons to transfer, and thus achieves an increased photocurrent.

4. CONCLUSIONS

In summary, an n-type metal−organic framework, PCN-222, was first and successfully developed as a simple and efficient "signal-on" photoelectrochemical probe for the detection of phosphates, due to its good electrical conductivity, special pore structure, and strong Zr−O−P affinity. The probe showed excellent selectivity, sensitivity, and stability, and the detection limit was as low as 1.964 nM, which was below the requirement of 6.4−320 μM for the detection of phosphate in the aqueous environment. A series of electrochemical and spectroscopic studies have proved that phosphate can bind to the ITO/PCN-222 electrode, which shortens the distance of the SCR while reducing the bandwidth and thus facilitates the transfer of photogenerated electrons across the energy band barrier to reduce O_2 in the electrolyte, producing an enhanced cathodic photocurrent signal. Moreover, the application of this PEC probe was well-validated in real water samples by the spiking method. This work provides a simple, rapid, and effective method for the detection of trace phosphate in water. At present, we are trying to use this probe for the detection of phosphate in biological systems. It may open up new avenues for further applications of MOF materials in environmental analysis and biomedicine.

■ ASSOCIATED CONTENT

Supporting Information

The Supporting Information is available free of charge at https://pubs.acs.org/doi/10.1021/acsami.2c04645.

Additional experimental details and results of characterizations using BET, TGA, SEM-EDS, PXRD, and FTIR, summary of reported detection methods of inorganic phosphate, and detection performance of ITO/PCN-222 to phosphate in real water samples (PDF)

■ AUTHOR INFORMATION

Corresponding Authors

Liping Lu − *Institute of Molecular Science, Key Laboratory of Chemical Biology and Molecular Engineering of the Education Ministry, Shanxi University, Taiyuan, Shanxi 030006, P. R. China; Key Laboratory of Materials for Energy Conversion and Storage of Shanxi Province, Shanxi University, Taiyuan, Shanxi 030006, P. R. China*; Email: luliping@sxu.edu.cn

Shengqian Ma − *Department of Chemistry, University of North Texas CHEM 305D, Denton, Texas 76201, United States*; orcid.org/0000-0002-1897-7069; Email: Shengqian.Ma@unt.edu

Sisi Feng − *Institute of Molecular Science, Key Laboratory of Chemical Biology and Molecular Engineering of the Education Ministry, Shanxi University, Taiyuan, Shanxi 030006, P. R. China; Key Laboratory of Materials for Energy Conversion and Storage of Shanxi Province, Shanxi University, Taiyuan, Shanxi 030006, P. R. China*; orcid.org/0000-0003-2357-2995; Email: ssfeng@sxu.edu.cn

Authors

Meirong Han − *Institute of Molecular Science, Key Laboratory of Chemical Biology and Molecular Engineering of the Education Ministry, Shanxi University, Taiyuan, Shanxi 030006, P. R. China*

Weijie Zhang − *Department of Chemistry, University of North Texas CHEM 305D, Denton, Texas 76201, United States*

Complete contact information is available at: https://pubs.acs.org/10.1021/acsami.2c04645

Notes

The authors declare no competing financial interest.

https://doi.org/10.1021/acsami.2c04645
ACS Appl. Mater. Interfaces 2022, 14, 28280−28288

■ ACKNOWLEDGMENTS

The authors thank the financial support of the Natural Science Foundation of China (Grant No. 21671124), the Fund for Shanxi "1331 Project" Key Innovative Research Team (1331KIRT), the Science and Technology Major Project of Shanxi (No. 202101030201022), and the Scientific Instrument Center of Shanxi University.

■ REFERENCES

(1) Ma, Y.; Zhang, Y.; Li, X.; Yang, P.; Yue, J. Y.; Jiang, Y.; Tang, B. Linker-Eliminated Nano Metal-Organic Framework Fluorescent Probe for Highly Selective and Sensitive Phosphate Ratiometric Detection in Water and Body Fluids. *Anal. Chem.* **2020**, *92*, 3722−3727.

(2) Li, L.; Zou, J. Y.; You, S. Y.; Liu, Y. W.; Cui, H. M.; Zhang, S. W. A Dual Luminescent Chemosensor Derived from a Europium(III) Metal-Organic Framework for Quantitative Detection of Phosphate Anions and Acetylacetone in Aqueous Solution. *Dyes Pigm.* **2020**, *173*, No. 108004.

(3) Han, L.; Liu, S. G.; Yang, Y. Z.; Fan, Y. Z.; Zhou, J.; Zhang, X. Y.; Li, N. B.; Luo, H. Q. A Lanthanide Coordination Polymer as a Ratiometric Fluorescent Probe for Rapid and Visual Sensing of Phosphate Based on the Target-Triggered Competitive Effect. *J. Mater. Chem. C* **2020**, *8*, 13063−13071.

(4) Das, A.; Das, S.; Trivedi, V.; Biswas, S. A Dual Functional MOF-Based Fluorescent Sensor for Intracellular Phosphate and Extracellular 4-Nitrobenzaldehyde. *Dalton Trans.* **2019**, *48*, 1332−1343.

(5) Gao, N.; Huang, J.; Wang, L.; Feng, J.; Huang, P.; Wu, F. Ratiometric Fluorescence Detection of Phosphate in Human Serum with a Metal-Organic Frameworks-Based Nanocomposite and Its Immobilized Agarose Hydrogels. *Appl. Surf. Sci.* **2018**, *459*, 686−692.

(6) Leclercq, T. M.; Pitson, S. M. Cellular Signalling by Sphingosine Kinase and Sphingosine 1-Phosphate. *IUBMB Life* **2006**, *58*, 467−472.

(7) Szyc, Ł.; Yang, M.; Elsaesser, T. Ultrafast Energy Exchange via Water-Phosphate Interactions in Hydrated DNA. *J. Phys. Chem. B* **2010**, *114*, 7951−7957.

(8) Levi, M.; Gratton, E.; Forster, I. C.; Hernando, N.; Wagner, C. A.; Biber, J.; Sorribas, V.; Murer, H. Mechanisms of phosphate transport. *Nat. Rev. Nephrol.* **2019**, *15*, 482−500.

(9) Zhang, W.; Xu, J.; Li, P.; Gao, X.; Zhang, W.; Wang, H.; Tang, B. Treatment of Hyperphosphatemia Based on Specific Interactions Between Phosphorus and Zr(iv) Active Centers of Nano-MOFs. *Chem. Sci.* **2018**, *9*, 7483−7487.

(10) Zhang, J.; Bian, Y.; Liu, D.; Zhu, Z.; Shao, Y.; Li, M. Detection of Phosphate in Human Blood Based on a Catalytic Hydrogen Wave at a Molybdenum Phosphide Modified Electrode. *Anal. Chem.* **2019**, *91*, 14666−14671.

(11) Zhang, Z.; Feng, J.; Huang, P.; Li, S.; Wu, F. Y. Ratiometric Fluorescent Detection of Phosphate in Human Serum with Functionalized Gold Nanoclusters Based on Chelation-Enhanced Fluorescence. *Sens. Actuators, B* **2019**, *298*, No. 126891.

(12) Asha, K. S.; Bhattacharjee, R.; Mandal, S. Complete Transmetalation in a Metal-Organic Framework by Metal Ion Metathesis in a Single Crystal for Selective Sensing of Phosphate Ions in Aqueous Media. *Angew. Chem., Int. Ed.* **2016**, *55*, 11528−11532.

(13) Bruce, J. I.; Dickins, R. S.; Govenlock, L. J.; Gunnlaugsson, T.; Lopinski, S.; Lowe, M. P.; Parker, D.; Peacock, R. D.; Perry, J. J. B.; Aime, S.; Botta, M. The Selectivity of Reversible Oxy-Anion Binding in Aqueous Solution at a Chiral Europium and Terbium Center: Signaling of Carbonate Chelation by Changes in the Form and Circular Polarization of Luminescence Emission. *J. Am. Chem. Soc.* **2000**, *122*, 9674−9684.

(14) Sun, S.; Chen, Q.; Sheth, S.; Ran, G.; Song, Q. Direct Electrochemical Sensing of Phosphate in Aqueous Solutions Based on Phase Transition of Calcium Phosphate. *ACS Sens.* **2020**, *5*, 541−548.

(15) Xu, K.; Kitazumi, Y.; Kano, K.; Sasaki, T.; Shirai, O. Fabrication of a Phosphate Ion Selective Electrode Based on Modified Molybdenum Metal. *Anal. Sci.* **2020**, *36*, 201−206.

(16) Zhu, J. M.; Shi, Y.; Zhu, X. Q.; Yang, Y.; Jiang, F. H.; Sun, C. J.; Zhao, W. H.; Han, X. T. Optofluidic Marine Phosphate Detection with Enhanced Absorption Using a Fabry-Perot Resonator. *Lab Chip* **2017**, *17*, 4025−4030.

(17) Cheng, C.; Zhang, R.; Wang, J.; Zhang, Y.; Xiong, S.; Huang, Y.; Yang, M. Porphyrinic Metal-Organic Framework Nanorod-Based Dual-Modal Nanoprobe for Sensing and Bioimaging of Phosphate. *ACS Appl. Mater. Interfaces* **2020**, *12*, 26391−26398.

(18) Khatua, S.; Choi, S. H.; Lee, J.; Kim, K.; Do, Y.; Churchill, D. G. Aqueous Fluorometric and Colorimetric Sensing of Phosphate Ions by a Fluorescent Dinuclear Zinc Complex. *Inorg. Chem.* **2009**, *48*, 2993−2999.

(19) Samy, R.; Faustino, P. J.; Adams, W.; Yu, L.; Khan, M. A.; Yang, Y. Development and Validation of An Ion Chromatography Method for the Determination of Phosphate-Binding of Lanthanum Carbonate. *J. Pharm. Biomed. Anal.* **2010**, *51*, 1108−1112.

(20) Luo, B.; Groenke, K.; Takors, R.; Wandrey, C.; Oldiges, M. Simultaneous Determination of Multiple Intracellular Metabolites in Glycolysis, Pentose Phosphate Pathway and Tricarboxylic Acid Cycle by Liquid Chromatography-Mass Spectrometry. *J. Chromatogr. A* **2007**, *1147*, 153−164.

(21) Guo, Z. X.; Cai, Q.; Yang, Z. Determination of Glyphosate and Phosphate in Water by Ion Chromatography-Inductively Coupled Plasma Mass Spectrometry Detection. *J. Chromatogr. A* **2005**, *1100*, 160−167.

(22) Yu, K.; Wei, T.; Li, Z.; Li, J.; Wang, Z.; Dai, Z. Construction of Molecular Sensing and Logic Systems Based on Site-Occupying Effect-Modulated MOF-DNA Interaction. *J. Am. Chem. Soc.* **2020**, *142*, 21267−21271.

(23) Chen, Q.; Sun, S.; Ran, G.; Wang, C.; Gu, W.; Song, Q. Electrochemical Detection of Phosphate Ion in Body Fluids with a Magnesium Phosphate Modified Electrode. *Anal. Sci.* **2021**, *37*, 1247−1252.

(24) Forano, C.; Farhat, H.; Mousty, C. Recent Trends in Electrochemical Detection of Phosphate in Actual Waters. *Curr. Opin. Electrochem.* **2018**, *11*, 55−61.

(25) Yang, Y.; Yan, W.; Wang, X.; Yu, L.; Zhang, J.; Bai, B.; Guo, C.; Fan, S. Development of a Molecularly Imprinted Photoelectrochemical Sensing Platform Based on NH_2-MIL-125(Ti)-TiO_2 Composite for the Sensitive and Selective Determination of Oxtetracycline. *Biosens. Bioelectron.* **2021**, *177*, No. 113000.

(26) Zang, Y.; Fan, J.; Ju, Y.; Xue, H.; Pang, H. Current Advances in Semiconductor Nanomaterial-Based Photoelectrochemical Biosensing. *Chem. - Eur. J.* **2018**, *24*, 14010−14027.

(27) Fan, L.; Zhang, C.; Shi, H.; Zhao, G. Design of a Simple and Novel Photoelectrochemical Aptasensor for Detection of 3,3′,4,4′-tetrachlorobiphenyl. *Biosens. Bioelectron.* **2019**, *124*−*125*, 8−14.

(28) Moumen, E.; Bazzi, L.; El Hankari, S. Metal-Organic Frameworks and their Composites for the Adsorption and Sensing of Phosphate. *Coord. Chem. Rev.* **2022**, *455*, No. 214376.

(29) Zhang, G. Y.; Zhuang, Y. H.; Shan, D.; Su, G. F.; Cosnier, S.; Zhang, X. J. Zirconium-Based Porphyrinic Metal-Organic Framework (PCN-222): Enhanced Photoelectrochemical Response and Its Application for Label-Free Phosphoprotein Detection. *Anal. Chem.* **2016**, *88*, 11207−11212.

(30) Xu, H. Q.; Hu, J.; Wang, D.; Li, Z.; Zhang, Q.; Luo, Y.; Yu, S. H.; Jiang, H. L. Visible-Light Photoreduction of CO_2 in a Metal-Organic Framework: Boosting Electron-Hole Separation via Electron Trap States. *J. Am. Chem. Soc.* **2015**, *137*, 13440−13443.

(31) Biswas, S.; Chen, Y.; Xie, Y.; Sun, X.; Wang, Y. Ultrasmall Au(0) Inserted Hollow PCN-222 MOF for The High-Sensitive Detection of Estradiol. *Anal. Chem.* **2020**, *92*, 4566−4572.

(32) Chen, Y.; Ma, S. Biomimetic Catalysis of Metal-Organic Frameworks. *Dalton Trans.* **2016**, *45*, 9744−9753.

(33) Jin, J. Porphyrin-Based Metal−Organic Framework Catalysts for Photoreduction of CO_2: Understanding the Effect of Node

https://doi.org/10.1021/acsami.2c04645
ACS Appl. Mater. Interfaces 2022, 14, 28280−28288

Connectivity and Linker Metalation on Activity. *New J. Chem.* **2020**, *44*, 15362−15368.
(34) Li, L.; Yu, X.; Xu, L.; Zhao, Y. Fabrication of a Novel Type Visible-Light-Driven Heterojunction Photocatalyst: Metal-Porphyrinic Metal Organic Framework Coupled with PW_{12}/TiO_2. *Chem. Eng. J.* **2020**, *386*, No. 123955.
(35) Zhao, Y.; Hou, S.; Liu, D.; Zhong, C. Effective Adsorption of Cefradine from Wastewater with a Stable Zirconium Metal−Organic Framework. *Ind. Eng. Chem. Res.* **2018**, *57*, 15132−15137.
(36) Tokalıoğlu, Ş.; Yavuz, E.; Demir, S.; Patat, Ş. Zirconium-Based Highly Porous Metal-Organic Framework (MOF-545) as an Efficient Adsorbent for Vortex Assisted-Solid Phase Extraction of Lead from Cereal, Beverage and Water Samples. *Food Chem.* **2017**, *237*, 707−715.
(37) Sarker, M.; Shin, S.; Jeong, J. H.; Jhung, S. H. Mesoporous Metal-Organic Framework PCN-222(Fe): Promising Adsorbent for Removal of Big Anionic and Cationic Dyes from Water. *Chem. Eng. J.* **2019**, *371*, 252−259.
(38) Oveisi, A. R.; Delarami, H. S.; Khajeh, M.; Mirjahanshahi, S.; Haghani, A.; Daliran, S.; Ghaffari-Moghaddam, M. Contributions of Metalloporphyrin Linkers and Zr_6 Nodes in Gas Adsorption on a Series of Bioinspired Zirconium-Based Metal-Organic Frameworks: A Computational Study. *J. Mol. Struct.* **2020**, *1204*, No. 127559.
(39) Moghaddam, Z. S.; Kaykhaii, M.; Khajeh, M.; Oveisi, A. R. PCN-222 Metal-Organic Framework: a Selective and Highly Efficient Sorbent for The Extraction of Aspartame from Gum, Juice, and Diet Soft Drink Before Its Spectrophotometric Determination. *BMC Chem.* **2020**, *14*, No. 19.
(40) Nazri, S.; Khajeh, M.; Oveisi, A. R.; Luque, R.; Rodríguez-Castellón, E.; Ghaffari-Moghaddam, M. Thiol-Functionalized PCN-222 MOF for Fast and Selective Extraction of Gold Ions from Aqueous Media. *Sep. Purif. Technol.* **2021**, *259*, No. 118197.
(41) Wang, S.; Chen, Y.; Wang, S.; Li, P.; Mirkin, C. A.; Farha, O. K. DNA-Functionalized Metal-Organic Framework Nanoparticles for Intracellular Delivery of Proteins. *J. Am. Chem. Soc.* **2019**, *141*, 2215−2219.
(42) He, J.; Wu, X.; Long, Z.; Hou, X. Fast and Sensitive Fluorescent and Visual Sensing of Cysteine Using Hg-Metalated PCN-222. *Microchem. J.* **2019**, *145*, 68−73.
(43) Chen, B.; Jiang, T.; Fu, H.; Qu, X.; Xu, Z.; Zheng, S. Ultrasensitive, Rapid and Selective Sensing of Hazardous Fluoride Ion in Aqueous Solution Using a Zirconium Porphyrinic Luminescent Metal-Organic Framework. *Anal. Chim. Acta* **2021**, *1145*, 95−102.
(44) Morris, W.; Volosskiy, B.; Demir, S.; Gandara, F.; McGrier, P. L.; Furukawa, H.; Cascio, D.; Stoddart, J. F.; Yaghi, O. M. Synthesis, Structure, and Metalation of Two New Highly Porous Zirconium Metal−Organic Frameworks. *Inorg. Chem.* **2012**, *51*, 6443−6445.
(45) Feng, D.; Gu, Z. Y.; Li, J. R.; Jiang, H. L.; Wei, Z.; Zhou, H. C. Zirconium-Metalloporphyrin PCN-222: Mesoporous Metal−Organic Frameworks with Ultrahigh Stability as Biomimetic Catalysts. *Angew. Chem., Int. Ed.* **2012**, *51*, 10307−10310.
(46) Ye, Y.; Huang, C.; Yang, J.; Li, Y.; Zhuang, Q.; Gu, J. Highly Selective and Rapid Detection of Pentachlorophenol in Aqueous Solution with Metalloporphyrinic MOFs. *Microporous Mesoporous Mater.* **2019**, *284*, 36−42.
(47) Xu, Z.; Meng, Q.; Cao, Q.; Xiao, Y.; Liu, H.; Han, G.; Wei, S.; Yan, J.; Wu, L. Selective Sensing of Copper Ions by Mesoporous Porphyrinic Metal-Organic Framework Nanoovals. *Anal. Chem.* **2020**, *92*, 2201−2206.
(48) Zhou, Q.; Li, G.; Chen, K.; Yang, H.; Yang, M.; Zhang, Y.; Wan, Y.; Shen, Y.; Zhang, Y. Simultaneous Unlocking Optoelectronic and Interfacial Properties of C_{60} for Ultrasensitive Immunosensing by Coupling to Metal-Organic Framework. *Anal. Chem.* **2020**, *92*, 983−990.
(49) Afzal, S.; Daoud, W. A.; Langford, S. J. Self-Cleaning Cotton by Porphyrin-Sensitized Visible-Light Photocatalysis. *J. Mater. Chem.* **2012**, *22*, 4083−4088.
(50) Smirnova, S. V.; Samarina, T. O.; Ilin, D. V.; Pletnev, I. V. Multielement Determination of Trace Heavy Metals in Water by Microwave-Induced Plasma Atomic Emission Spectrometry after Extraction in Unconventional Single-Salt Aqueous Biphasic System. *Anal. Chem.* **2018**, *90*, 6323−6331.
(51) Wang, J.; Chen, Y.; Shen, Y.; Liu, S.; Zhang, Y. Coupling Polymorphic Nanostructured Carbon Nitrides into an Isotype Heterojunction with Boosted Photocatalytic H_2 Evolution. *Chem. Commun.* **2017**, *53*, 2978−2981.
(52) Zhao, Y.; Dong, Y.; Lu, F.; Ju, C.; Liu, L.; Zhang, J.; Zhang, B.; Feng, Y. Coordinative Integration of a Metal-Porphyrinic Framework and TiO_2 Nanoparticles for the Formation of Composite Photocatalysts with Enhanced Visible-Light-Driven Photocatalytic Activities. *J. Mater. Chem. A* **2017**, *5*, 15380−15389.
(53) Urbani, M.; Grätzel, M.; Nazeeruddin, M. K.; Torres, T. Meso-Substituted Porphyrins for Dye-Sensitized Solar Cells. *Chem. Rev.* **2014**, *114*, 12330−12396.
(54) Ikeda, A.; Nakasu, M.; Ogasawara, S.; Nakanishi, H.; Nakamura, M.; Kikuchi, J.-i. Photoelectrochemical Sensor with Porphyrin-Deposited Electrodes for Determination of Nucleotides in Water. *Org. Lett.* **2009**, *11*, 1163−1166.
(55) Yang, J.; Dai, Y.; Zhu, X.; Wang, Z.; Li, Y.; Zhuang, Q.; Shi, J.; Gu, J. Metal−Organic Frameworks with Inherent Recognition Sites for Selective Phosphate Sensing through their Coordination-Induced Fluorescence Enhancement Effect. *J. Mater. Chem. A* **2015**, *3*, 7445−7452.
(56) Gu, Y.; Xie, D.; Ma, Y.; Qin, W.; Zhang, H.; Wang, G.; Zhang, Y.; Zhao, H. Size Modulation of Zirconium-Based Metal Organic Frameworks for Highly Efficient Phosphate Remediation. *ACS Appl. Mater. Interfaces* **2017**, *9*, 32151−32160.
(57) Zhu, X.; Gu, J.; Wang, Y.; Li, B.; Li, Y.; Zhao, W.; Shi, J. Inherent Anchorages in UiO-66 Nanoparticles for Efficient Capture of Alendronate and Its Mediated Release. *Chem. Commun.* **2014**, *50*, 8779−8782.
(58) Zhu, X.; Li, B.; Yang, J.; Li, Y.; Zhao, W.; Shi, J.; Gu, J. Effective Adsorption and Enhanced Removal of Organophosphorus Pesticides from Aqueous Solution by Zr-based MOFs of UiO-67. *ACS Appl. Mater. Interfaces* **2015**, *7*, 223−231.
(59) Peng, M.; Guan, G.; Deng, H.; Han, B.; Tian, C.; Zhuang, J.; Xu, Y.; Liu, W.; Lin, Z. PCN-224/rGO Nanocomposite Based Photoelectrochemical Sensor with Intrinsic Recognition Ability for Efficient *p*-arsanilic Acid Detection. *Environ. Sci.: Nano* **2019**, *6*, 207−215.
(60) Xie, D.; Gu, Y.; Wang, H.; Wang, Y.; Qin, W.; Wang, G.; Zhang, H.; Zhang, Y. Enhanced Fluoride Removal by Hierarchically Porous Carbon Foam Monolith with High Loading of UiO-66. *J. Colloid Interface Sci.* **2019**, *542*, 269−280.
(61) Chen, Y. Z.; Wang, Z. U.; Wang, H.; Lu, J.; Yu, S. H.; Jiang, H. L. Singlet Oxygen-Engaged Selective Photo-Oxidation over Pt Nanocrystals/Porphyrinic MOF: The Roles of Photothermal Effect and Pt Electronic State. *J. Am. Chem. Soc.* **2017**, *139*, 2035−2044.
(62) Fu, B.; Zhang, Z. Sensitive and Site-Selective Determination of Phosphorylated Peptides with a Ratiometric Photoelectrochemical Strategy. *Anal. Chem.* **2019**, *91*, 14829−14833.
(63) Yang, Y.; Xu, D.; Wu, Q.; Diao, P. Cu_2O/CuO Bilayered Composite as a High-Efficiency Photocathode for Photoelectrochemical Hydrogen Evolution Reaction. *Sci. Rep.* **2016**, *6*, No. 35158.
(64) Yu, D.; Li, L.; Wu, M.; Crittenden, J. C. Enhanced Photocatalytic Ozonation of Organic Pollutants Using an Iron-Based Metal-Organic Framework. *Appl. Catal., B* **2019**, *251*, 66−75.

https://doi.org/10.1021/acsami.2c04645
ACS Appl. Mater. Interfaces 2022, 14, 28280−28288